

THE SPREAD OF METALS INTO THE LOW-REDSHIFT INTERGALACTIC MEDIUM

CAMERON T. PRATT,¹ JOHN T. STOCKE,¹ BRIAN A. KEENEY,¹ AND CHARLES W. DANFORTH¹

¹*Center for Astrophysics and Space Astronomy, Department of Astrophysical and Planetary Sciences, University of Colorado, 389 UCB, Boulder, CO 80309, USA*

ABSTRACT

We investigate the association between galaxies and metal-line and metal-free absorbers in the local universe ($z < 0.16$) using a large compilation of FUV spectra of bright AGN targets observed with the Cosmic Origins Spectrograph aboard the *Hubble Space Telescope*. In this homogeneous sample of 24 O VI detections ($Z \geq 0.1 Z_{\odot}$) and 25 non-detections, the maximum distance O VI extends from galaxies of various luminosities is ~ 0.6 Mpc, or $\sim 5 R_{\text{vir}}$, confirming and refining earlier results. This is an important value that must be matched by numerical simulations, which input the strength of galactic winds at the sub-grid level. We present evidence that the primary contributors to the spread of metals into the circum- and intergalactic media are $L < L^*$ galaxies. The maximum distances that metals are transported from these galaxies is comparable to the size of a small, spiral-rich group of galaxies. This suggests that, while rather pristine intergalactic material may accrete onto these groups where it can mix with metal-bearing clouds, the metals produced by the group galaxies may not leave the group, creating a nearly “closed box” for galactic evolution.

Keywords: quasars: absorption lines — galaxies: halos — intergalactic medium — galaxies: abundances — galaxies: evolution

1. INTRODUCTION

Models of galactic evolution must incorporate the accretion of low-metallicity gas ($Z \sim 0.1 Z_{\odot}$) from the ambient intergalactic medium (IGM; e.g., Oppenheimer et al. 2012) both in order to resolve the ‘‘G-dwarf problem’’ (Pagel 2009) and to maintain the high star formation rates seen in late-type galaxies like the Milky Way (Binney & Tremaine 1987). The modest metallicity of this accreting gas suggests a source within nearby, low-mass galaxies although the mass range of the source galaxies is not known specifically. Ultimately, a mixture of outflows and accretion composes the massive, gaseous halos that surround most late-type galaxies, known as the circumgalactic medium (CGM; Tumlinson et al. 2011; Stocke et al. 2013; Werk et al. 2014; Burchett et al. 2016; Keeney et al. 2017).

Some studies suggest that the CGM extends from the disk of a star-forming galaxy to its ‘‘virial radius’’ (R_{vir} ; Stocke et al. 2013; Shull 2014), which is the distance a galaxy has gravitational influence on its surroundings. At least one recent study presents evidence that the CGM does not extend much beyond $1/2 R_{\text{vir}}$ (Prochaska et al. 2017), but Shull (2014) argues that parts of the CGM can include unbound outflows beyond R_{vir} . Simulations suggest that the amount of gas and metals that escapes is a strong function of both galaxy mass and redshift, with ‘‘gusty’’ winds at high- z calming down to bound ‘‘galactic fountains’’ for the most massive halos at $z < 1$ (Muratov et al. 2015, 2017; Hayward & Hopkins 2017).

The boundary between the CGM and IGM is rather ambiguous, especially for galaxies of widely differing escape velocities. AGN absorption-line observations support this premise because there are no strong changes in H I absorber properties, including covering factor and mean H I column density, which decline monotonically in the $1\text{--}5 R_{\text{vir}}$ range (Stocke et al. 2013). However, metal-bearing absorbers decline rapidly away from the nearest galaxies (e.g., Chen et al. 1998; Finn et al. 2016; Burchett et al. 2016) and have yet to be detected in galaxy voids (Stocke et al. 2007).

Simulations by Oppenheimer et al. (2012) suggest that it is primarily low-mass galaxies whose supernova-driven winds enrich the IGM with metals, because winds produced by very massive galaxies ($M \geq 10^{11} M_{\odot}$) may be incapable of breaching their surrounding gaseous halos (Côté et al. 2012; Hayward & Hopkins 2017). Instead, these outflows may fall back onto galactic disks and re-ignite star formation (e.g., Veilleux, Cecil, & Bland-Hawthorn 2005), as in our own galaxy (Keeney et al. 2006; Bordoloi et al. 2017).

When large-scale simulations (e.g., Davé et al. 1999, 2011; Cen & Ostriker 1999) place galactic winds in a cosmological context, the strength of these winds and their full range of extent often are input at a sub-pixel level (so-called sub-grid physics, but see recent, high-resolution simulations by the FIRE collaboration; Hopkins et al. 2016) so that the extent to

which metals are transported away from their source galaxy is not determined *a priori* in most simulations. Thus, this maximum extent provides both an observational bound for a galaxy’s CGM and a constraint on galactic wind modeling within cosmological simulations.

In this paper we present an estimate of the maximum distance winds propagate away from galaxies using low-redshift absorption found in the far-ultraviolet (FUV) spectra of bright AGN obtained with the *Cosmic Origins Spectrograph* (COS) aboard the *Hubble Space Telescope* (HST), in conjunction with an extensive database of low- z galaxy positions and redshifts near these sight lines (Stocke et al. 2013; Keeney et al. 2017, B. Keeney et al. 2017, in preparation). Since O VI (1032, 1038 Å) exhibits the greatest extent away from galaxies of any of the ions detected in absorption in the FUV (Prochaska et al. 2011; Stocke et al. 2013; Keeney et al. 2017), this study uses only the O VI doublet.

The present O VI study expands upon and updates similar O VI work by Stocke et al. (2006), in which a smaller sample of absorbers was used to determine that metals spread no more than ~ 800 kpc from L^* galaxies (see also Johnson, Chen, & Mulchaey 2015; Finn et al. 2016). In Section 2 the absorption-line and galaxy survey data are described; Section 3 presents the results and Section 4 provides a summary of our results and conclusions.

2. ABSORBER AND GALAXY SAMPLES

2.1. H I and O VI Absorber Sample

This search for galaxy-absorber associations uses the largest survey of the low- z IGM to date (Danforth et al. 2016, with updated column densities computed for some absorbers in Keeney et al. 2017). These authors used HST/COS FUV spectra to construct an absorber sample along 82 AGN sight lines in the redshift range $0.05 < z < 0.75$. However, O VI falls in the COS bandpass only at $z \gtrsim 0.11$. Since the galaxy redshift surveys employed are naturally weighted towards $z \leq 0.1$, previous data from the *Far-Ultraviolet Spectroscopic Explorer* (FUSE) satellite of a few very bright AGN were incorporated to expand the range of coverage to more low- z O VI absorbers. We refer the reader to Danforth et al. (2016) and Keeney et al. (2017) for a detailed discussion of the data handling.

Only ‘‘clean’’ detections and non-detections of O VI were employed; meaning, the spectra exhibit no intervening lines (e.g. interstellar transitions or redshifted Ly α lines) at the same wavelengths of O VI. Also, the O VI doublet is required to be sampled at high signal-to-noise ($S/N > 15$), allowing the detection of O VI at $N_{\text{O VI}} \gtrsim 2 \times 10^{13} \text{ cm}^{-2}$, or upper limits below that level. While the S/N of the COS FUV spectra is not uniform, these high- S/N data allow a detection of metal-enriched absorbers in the metallicity range $Z \geq 0.1 Z_{\odot}$ (Keeney et al. 2017) based upon CLOUDY modeling (Fer-

land et al. 1998). Starting with a Ly α absorption-line redshift there were 24 detections and 25 non-detections in O VI at $z \leq 0.16$.

Danforth et al. (2016) and Keeney et al. (2017) list the absorbers used in this survey and provide spectra, velocities and equivalent widths or limits for H I and common metal-line species, including C II, C III, C IV, Si II, Si III, Si IV, and O VI, when they occur within the *HST*/COS or *FUSE* bandpasses. Since all of these absorbers include at least H I Ly α , absorber velocities for Ly α are used and have a velocity error of $\pm 15 \text{ km s}^{-1}$ due to the absolute wavelength uncertainty of the *HST*/COS G130M and G160M gratings (Green et al. 2012). Somewhat larger velocity errors are quoted for some absorbers in Danforth et al. (2016) and Keeney et al. (2017) for Ly α lines with complex line profiles.

2.2. Galaxy Redshift Surveys

The galaxy data were obtained from four ground-based telescopes: the Sloan Digital Sky Survey (SDSS) spectroscopic sample (DR12; Alam et al. 2015) and multi-object spectroscopy (MOS) from the 3.5-m Wisconsin-Indiana-Yale-NOAO (WIYN) telescope at Kitt Peak National Observatory, the 3.9-m Anglo-Australian Telescope (AAT), and the 4-m Blanco telescope at Cerro Tololo Inter-American Observatory. While the SDSS spectroscopic survey is relatively shallow ($m_r \leq 17.8$), it provides large-angle coverage which is unmatched in the south, where we relied upon a compilation of various galaxy redshift surveys including the 2dF (Colless et al. 2007) and 6dF (Jones et al. 2009) surveys. These wide-field surveys were complemented by much deeper ($m_g \leq 20$) MOS, primarily obtained at WIYN with the HYDRA spectrograph. Individual field completeness levels vary but are typically $> 90\%$ out to completeness impact parameters (ρ_{lim}) of 0.5-2 Mpc for most absorbers; details of the observational process, data reduction and analysis, and redshift determination are presented in B. Keeney et al. (2017, in preparation).

There are several reasons why the completeness for obtaining measurable redshifts does not reach 100%, including an inability to place fibers on galaxies separated by $\leq 20''$ on the sky, and very diffuse galaxies whose spectrum is inconclusive despite a total magnitude brighter than a given completeness limit (L_{lim}) at the absorber redshift. Table 1 presents the completeness levels of our galaxy surveys for each absorber. A completeness level of $\geq 90\%$ is required herein as in our first study Stocke et al. (2006). Blank entries are not complete to L_{lim} at $\geq 90\%$, and so are not part of this survey. Absorbers with entries of “SDSS” are complete to $\geq 94\%$ based on the limits of DR12 (see Alam et al. 2015, B. Keeney et al. 2017, in preparation).

2.3. Nearest Galaxy Data

Although redshift accuracies vary somewhat depending on the intrinsic galaxy spectrum (e.g., pure emission-line, emission plus absorption line, or pure absorption line), these errors are typically $\pm 30 \text{ km s}^{-1}$ as determined for objects which were observed multiple times in our program (B. Keeney et al. 2017, in preparation). We *de facto* assume that any galaxy within $\pm 1000 \text{ km s}^{-1}$ of the absorber velocity could be associated with the absorber, but compute a three-dimensional distance between each of these nearby galaxies and the absorbers by assuming a “retarded Hubble flow” model. Under this assumption, the line-of-sight distance between absorber and galaxy (D_{los}) is zero if the galaxy-absorber velocity difference, $|\Delta v| \leq 400 \text{ km s}^{-1}$ and is otherwise determined using “pure Hubble flow”; i.e., $D_{\text{los}} = (|\Delta v| - 400 \text{ km s}^{-1})/H_0$.

While the “retarded velocity” limit is arbitrary, this choice is based upon the rotation speed of an $L > L^*$ galaxy. Other research groups (e.g., Prochaska et al. 2011) have assumed much larger values ($\pm 1000 \text{ km s}^{-1}$), which decreases the three-dimensional absorber-galaxy distance significantly in cases where $400 \text{ km s}^{-1} < |\Delta v| < 1000 \text{ km s}^{-1}$. Only a few galaxies with $|\Delta v| > 400 \text{ km s}^{-1}$ are identified as nearest galaxies by this study, mostly for $L > L^*$ galaxies (5 cases).

We also consider galaxy distances in units of the nearest galaxy’s virial radius, R_{vir} . Virial radii (and halo masses) are determined from the galaxy’s rest-frame *g*-band luminosity as described in Stocke et al. (2013) and Keeney et al. (2017). Figure 1 of Stocke et al. (2013) shows the function adopted in comparison with different scaling relationships used by other groups. For $L > L^*$ galaxies, these virial radii are approximately a factor of two smaller than the values assumed by Prochaska et al. (2011), or those used by the COS-Halos team (e.g., Werk et al. 2014). Scrutiny of several dozen, low- z *HST*/COS-discovered absorbers finds that the identification of an absorber with a specific galaxy is robust out to $\rho \lesssim 1.4 R_{\text{vir}}$ (Keeney et al. 2017).

Table 2 presents the basic data used in this study, in which the third column identifies the O VI detections and non-detections. The remaining columns (keyed to the limiting galaxy luminosity, L_{lim}) list the nearest galaxy luminosity, L , and three-dimensional absorber-galaxy physical distance, D and distances scaled by R_{vir} . The nearest “physical galaxy” often is different from the nearest galaxy when distances are scaled by R_{vir} . Columns 4-7 use all available data regardless of galaxy luminosity. Columns 8-11, 12-15, and 16-19 use all galaxies with $L \geq 0.25 L^*$, $L \geq 0.5 L^*$, and $L \geq L^*$ respectively. Absorber regions that were not surveyed deeply enough to reach the limiting luminosities given at the top have no data shown.

Table 1. Galaxy Survey Completeness Limits Surrounding IGM Absorbers

| Sight Line | z_{abs} | $L_{\text{lim}} = 0.25L^*$ | | $L_{\text{lim}} = 0.5L^*$ | | $L_{\text{lim}} = L^*$ | |
|-----------------|------------------|----------------------------|--------------|---------------------------|--------------|------------------------|--------------|
| | | ρ_{lim} | Completeness | ρ_{lim} | Completeness | ρ_{lim} | Completeness |
| | | (Mpc) | (%) | (Mpc) | (%) | (Mpc) | (%) |
| IES 1028+511 | 0.14057 | ... | ... | 3.00 | 100% | 3.00 | 100% |
| IES 1553+113 | 0.10224 | ... | ... | ... | ... | SDSS | SDSS |
| 3C 263 | 0.06328 | 1.48 | 100% | SDSS | SDSS | SDSS | SDSS |
| 3C 263 | 0.06352 | 1.48 | 100% | SDSS | SDSS | SDSS | SDSS |
| 3C 263 | 0.11309 | 2.49 | 94.03% | 2.49 | 100% | SDSS | SDSS |
| 3C 263 | 0.11392 | 2.51 | 92.65% | 2.51 | 100% | SDSS | SDSS |
| 3C 263 | 0.12232 | 2.67 | 94.38% | 2.67 | 100% | SDSS | SDSS |
| 3C 263 | 0.14075 | ... | ... | 3.01 | 100% | 3.01 | 100% |
| FBQS J1010+3003 | 0.12833 | 2.78 | 95.73% | 2.78 | 100% | 2.78 | 100% |
| H1821+643 | 0.12120 | 2.65 | 93.07% | 2.65 | 96.15% | SDSS | SDSS |
| HE 0153-4520 | 0.13210 | 2.85 | 92.31% | 2.85 | 90.32% | 2.85 | 96.67% |
| HE 0226-4110 | 0.06087 | 1.42 | 100% | 1.42 | 100% | 1.42 | 100% |
| PG 0953+414 | 0.06809 | 1.58 | 100% | SDSS | SDSS | SDSS | SDSS |
| PG 1001+291 | 0.11346 | 2.50 | 94.87% | 2.50 | 96.15% | SDSS | SDSS |
| PG 1001+291 | 0.13744 | ... | ... | 2.95 | 95.92% | ... | ... |
| PG 1048+342 | 0.14471 | ... | ... | 3.08 | 95% | 2.00 | 100% |
| PG 1116+215 | 0.13853 | ... | ... | ... | ... | ... | ... |
| PG 1216+069 | 0.12360 | 1.35 | 95.24% | 2.15 | 92.86% | 2.15 | 100% |
| PG 1216+069 | 0.12389 | 1.35 | 95.24% | 2.16 | 92.86% | 2.16 | 100% |
| PG 1216+069 | 0.12478 | 1.36 | 95.45% | 2.17 | 93.33% | 2.17 | 100% |
| PG 1216+069 | 0.13507 | ... | ... | 1.89 | 90.91% | 2.32 | 100% |
| PG 1222+216 | 0.15554 | ... | ... | ... | ... | 2.78 | 100% |
| PG 1222+216 | 0.15580 | ... | ... | ... | ... | 2.78 | 100% |
| PG 1259+593 | 0.00763 | SDSS | SDSS | SDSS | SDSS | SDSS | SDSS |
| PG 1259+593 | 0.04611 | SDSS | SDSS | SDSS | SDSS | SDSS | SDSS |
| PG 1259+593 | 0.08935 | 2.02 | 91.43% | ... | ... | SDSS | SDSS |
| PG 1424+240 | 0.11582 | ... | ... | 2.54 | 100% | SDSS | SDSS |
| PG 1424+240 | 0.12134 | ... | ... | 2.65 | 95.45% | SDSS | SDSS |
| PG 1424+240 | 0.12776 | ... | ... | 2.49 | 90% | 2.77 | 100% |
| PG 1424+240 | 0.14679 | ... | ... | 2.65 | 93.55% | 3.12 | 100% |
| PG 1424+240 | 0.14714 | ... | ... | 2.65 | 93.55% | 3.12 | 100% |
| PG 1626+554 | 0.09382 | 0.84 | 90.91% | 0.84 | 100% | SDSS | SDSS |
| PHL 1811 | 0.07348 | 1.70 | 97.78% | 1.70 | 100% | 1.70 | 100% |

Table 1 continued

Table 1 (*continued*)

| Sight Line | z_{abs} | $L_{\text{lim}} = 0.25L^*$ | | $L_{\text{lim}} = 0.5L^*$ | | $L_{\text{lim}} = L^*$ | |
|--------------|------------------|------------------------------|---------------------|------------------------------|---------------------|------------------------------|---------------------|
| | | ρ_{lim} (Mpc) | Completeness (%) | ρ_{lim} (Mpc) | Completeness (%) | ρ_{lim} (Mpc) | Completeness (%) |
| PHL 1811 | 0.07777 | 1.78 | 98.11% | 1.78 | 100% | 1.78 | 100% |
| PHL 1811 | 0.08084 | 1.85 | 98.44% | 1.85 | 100% | 1.85 | 100% |
| PHL 1811 | 0.12049 | 1.05 | 92.31% | 2.63 | 98.65% | 2.63 | 100% |
| PHL 1811 | 0.12071 | 1.05 | 92.31% | 2.64 | 98.65% | 2.64 | 100% |
| PHL 1811 | 0.13229 | 1.14 | 92.59% | 2.85 | 96.84% | 2.85 | 100% |
| PHL 1811 | 0.13547 | 1.17 | 92.59% | 2.91 | 96.94% | 2.91 | 100% |
| PKS 0405–123 | 0.09180 | 1.87 | 100% | 1.87 | 100% | 1.87 | 100% |
| PKS 0405–123 | 0.09655 | 1.95 | 91.67% | 1.95 | 100% | 1.95 | 100% |
| PKS 2005–489 | 0.01695 | ... | ... | ... | ... | ... | ... |
| PKS 2005–489 | 0.06499 | 0.15 | 100% | 0.15 | 100% | 0.15 | 100% |
| Q1230+0115 | 0.07770 | 1.78 | 100% | SDSS | SDSS | SDSS | SDSS |
| Q1230+0115 | 0.07807 | 1.79 | 100% | SDSS | SDSS | SDSS | SDSS |
| SBS 1122+594 | 0.11322 | 2.50 | 93.48% | 2.25 | 93.75% | SDSS | SDSS |
| SBS 1122+594 | 0.14315 | ... | ... | 3.05 | 93.65% | 1.52 | 100% |
| SBS 1122+594 | 0.15545 | ... | ... | 3.27 | 93.75% | 2.94 | 92.31% |
| Ton 580 | 0.13396 | 2.88 | 100% | 2.88 | 100% | 2.88 | 100% |

Table 2. Distances from Absorbers to their Nearest Galaxies

| Sight Line | z_{abs} | O VI | No Luminosity Limit | | | | | | $L_{\text{lim}} = 0.25 L^*$ | | | | | | $L_{\text{lim}} = 0.5 L^*$ | | | | | | $L_{\text{lim}} = L^*$ | | | | | |
|-----------------|------------------|------|---------------------|-------|----------------------------|-------|----------|-------|-----------------------------|-------|----------|-------|----------------------------|-------|----------------------------|-------|----------------------------|-------|----------|-------|----------------------------|-------|----------|-------|----------------------------|-------|
| | | | Physical | | Scaled by R_{vir} | | Physical | | Scaled by R_{vir} | | Physical | | Scaled by R_{vir} | | Physical | | Scaled by R_{vir} | | Physical | | Scaled by R_{vir} | | Physical | | Scaled by R_{vir} | |
| | | | L | D | L | D | L | D | L | D | L | D | L | D | L | D | L | D | L | D | L | D | L | D | L | D |
| IES 1028+511 | 0.14057 | n | 0.328 | 1.53 | 1.94 | 9.65 | ... | ... | ... | ... | 1.94 | 2.19 | 1.94 | 9.65 | 1.94 | 2.19 | 1.94 | 9.65 | 1.94 | 2.19 | 1.94 | 9.65 | 1.94 | 2.19 | 1.94 | 9.65 |
| IES 1553+113 | 0.10224 | n | 0.193 | 1.45 | 1.15 | 11.9 | ... | ... | ... | ... | ... | ... | ... | ... | ... | ... | ... | ... | ... | ... | ... | ... | ... | ... | ... | ... |
| 3C 263 | 0.06328 | y | 0.283 | 0.064 | 0.283 | 0.538 | 0.283 | 0.064 | 0.283 | 0.538 | 0.283 | 0.064 | 0.283 | 0.538 | 0.283 | 0.064 | 0.283 | 0.538 | 0.283 | 0.064 | 0.283 | 0.538 | 0.283 | 0.064 | 0.283 | 0.538 |
| 3C 263 | 0.06352 | y | 0.283 | 0.064 | 0.283 | 0.538 | 0.283 | 0.064 | 0.283 | 0.538 | 0.283 | 0.064 | 0.283 | 0.538 | 0.283 | 0.064 | 0.283 | 0.538 | 0.283 | 0.064 | 0.283 | 0.538 | 0.283 | 0.064 | 0.283 | 0.538 |
| 3C 263 | 0.11309 | n | 0.368 | 0.352 | 0.368 | 2.69 | 0.368 | 0.352 | 0.368 | 2.69 | 0.368 | 0.352 | 0.368 | 2.69 | 0.368 | 0.352 | 0.368 | 2.69 | 0.368 | 0.352 | 0.368 | 2.69 | 0.368 | 0.352 | 0.368 | 2.69 |
| 3C 263 | 0.11392 | y | 0.368 | 0.354 | 0.368 | 2.70 | 0.368 | 0.354 | 0.368 | 2.70 | 0.368 | 0.354 | 0.368 | 2.70 | 0.368 | 0.354 | 0.368 | 2.70 | 0.368 | 0.354 | 0.368 | 2.70 | 0.368 | 0.354 | 0.368 | 2.70 |
| 3C 263 | 0.12232 | n | 0.430 | 1.11 | 0.430 | 8.11 | 0.430 | 1.11 | 0.430 | 8.11 | 0.430 | 1.11 | 0.430 | 8.11 | 0.430 | 1.11 | 0.430 | 8.11 | 0.430 | 1.11 | 0.430 | 8.11 | 0.430 | 1.11 | 0.430 | 8.11 |
| 3C 263 | 0.14075 | y | 1.87 | 0.622 | 1.87 | 2.79 | ... | ... | ... | ... | ... | ... | ... | ... | ... | ... | ... | ... | ... | ... | ... | ... | ... | ... | ... | ... |
| FBQS J1010+3003 | 0.12833 | n | 0.235 | 0.529 | 1.49 | 3.18 | 1.49 | 0.658 | 1.49 | 3.18 | 1.49 | 0.658 | 1.49 | 3.18 | 1.49 | 0.658 | 1.49 | 3.18 | 1.49 | 0.658 | 1.49 | 3.18 | 1.49 | 0.658 | 1.49 | 3.18 |
| H1821+643 | 0.12120 | y | 0.776 | 0.159 | 0.776 | 0.952 | 0.776 | 0.159 | 0.776 | 0.952 | 0.776 | 0.159 | 0.776 | 0.952 | 0.776 | 0.159 | 0.776 | 0.952 | 0.776 | 0.159 | 0.776 | 0.952 | 0.776 | 0.159 | 0.776 | 0.952 |
| HE 0153-4520 | 0.13210 | y | 0.093 | 2.02 | 1.02 | 14.0 | 0.440 | 2.04 | 1.02 | 14.0 | 0.440 | 2.04 | 1.02 | 14.0 | 0.440 | 2.04 | 1.02 | 14.0 | 0.440 | 2.04 | 1.02 | 14.0 | 0.440 | 2.04 | 1.02 | 14.0 |
| HE 0226-4110 | 0.06087 | n | 0.287 | 0.352 | 0.287 | 2.93 | 0.287 | 0.352 | 0.287 | 2.93 | 0.287 | 0.352 | 0.287 | 2.93 | 0.287 | 0.352 | 0.287 | 2.93 | 0.287 | 0.352 | 0.287 | 2.93 | 0.287 | 0.352 | 0.287 | 2.93 |
| PG 0953+414 | 0.06809 | y | 0.892 | 0.611 | 0.892 | 3.49 | 0.892 | 0.611 | 0.892 | 3.49 | 0.892 | 0.611 | 0.892 | 3.49 | 0.892 | 0.611 | 0.892 | 3.49 | 0.892 | 0.611 | 0.892 | 3.49 | 0.892 | 0.611 | 0.892 | 3.49 |
| PG 1001+291 | 0.11346 | n | 0.225 | 0.816 | 1.01 | 6.08 | 0.324 | 0.883 | 1.01 | 6.08 | 0.324 | 0.883 | 1.01 | 6.08 | 0.324 | 0.883 | 1.01 | 6.08 | 0.324 | 0.883 | 1.01 | 6.08 | 0.324 | 0.883 | 1.01 | 6.08 |
| PG 1001+291 | 0.13744 | n | 0.132 | 0.055 | 0.132 | 0.585 | ... | ... | ... | ... | ... | ... | ... | ... | ... | ... | ... | ... | ... | ... | ... | ... | ... | ... | ... | ... |
| PG 1048+342 | 0.14471 | n | 0.364 | 0.410 | 0.364 | 3.15 | ... | ... | ... | ... | ... | ... | ... | ... | ... | ... | ... | ... | ... | ... | ... | ... | ... | ... | ... | ... |
| PG 1116+215 | 0.13853 | y | 1.76 | 0.139 | 1.76 | 0.632 | ... | ... | ... | ... | ... | ... | ... | ... | ... | ... | ... | ... | ... | ... | ... | ... | ... | ... | ... | ... |
| PG 1216+069 | 0.12360 | y | 0.657 | 0.094 | 0.657 | 0.595 | 0.657 | 0.094 | 0.657 | 0.595 | 0.657 | 0.094 | 0.657 | 0.595 | 0.657 | 0.094 | 0.657 | 0.595 | 0.657 | 0.094 | 0.657 | 0.595 | 0.657 | 0.094 | 0.657 | 0.595 |
| PG 1216+069 | 0.12389 | y | 0.657 | 0.094 | 0.657 | 0.595 | 0.657 | 0.094 | 0.657 | 0.595 | 0.657 | 0.094 | 0.657 | 0.595 | 0.657 | 0.094 | 0.657 | 0.595 | 0.657 | 0.094 | 0.657 | 0.595 | 0.657 | 0.094 | 0.657 | 0.595 |
| PG 1216+069 | 0.12478 | y | 0.657 | 0.094 | 0.657 | 0.595 | 0.657 | 0.094 | 0.657 | 0.595 | 0.657 | 0.094 | 0.657 | 0.595 | 0.657 | 0.094 | 0.657 | 0.595 | 0.657 | 0.094 | 0.657 | 0.595 | 0.657 | 0.094 | 0.657 | 0.595 |
| PG 1216+069 | 0.13507 | n | 1.38 | 0.758 | 1.38 | 3.75 | ... | ... | ... | ... | ... | ... | ... | ... | ... | ... | ... | ... | ... | ... | ... | ... | ... | ... | ... | ... |
| PG 1222+216 | 0.15554 | n | 0.646 | 0.498 | 0.646 | 3.17 | ... | ... | ... | ... | ... | ... | ... | ... | ... | ... | ... | ... | ... | ... | ... | ... | ... | ... | ... | ... |
| PG 1222+216 | 0.15580 | n | 0.646 | 0.498 | 0.646 | 3.17 | ... | ... | ... | ... | ... | ... | ... | ... | ... | ... | ... | ... | ... | ... | ... | ... | ... | ... | ... | ... |
| PG 1259+593 | 0.00763 | n | 0.085 | 0.474 | 0.770 | 3.51 | 0.770 | 0.586 | 0.770 | 3.51 | 0.770 | 0.586 | 0.770 | 3.51 | 0.770 | 0.586 | 0.770 | 3.51 | 0.770 | 0.586 | 0.770 | 3.51 | 0.770 | 0.586 | 0.770 | 3.51 |

Table 2 continued

3. THE SPREAD OF O VI AROUND LOW-Z GALAXIES

The most straightforward way to examine the spread of O VI from galaxies is through [Figure 1](#) which shows the 24 O VI detections and 25 O VI non-detections in double-sided histograms. The top histogram shows that O VI spreads no more than the 750 kpc bin from the nearest galaxy; the specific largest value is 620 kpc. The median luminosity of the galaxy physically nearest to a metal-enriched IGM absorbers is $0.61 L^*$, while the median of all galaxies nearest to absorbers in units of R_{vir} is $0.66 L^*$. Due to the large variation in nearest galaxy luminosities and thus virial radii, the metal spread extends to as much as $5 R_{\text{vir}}$ in some cases, leaving little doubt that the most remote absorbers are unbound gravitationally from the nearest galaxy.

However, one O VI detection (in the HE0153-4520 sight line at $z_{\text{abs}} = 0.13210$, and indicated in green in [Figure 1](#)) is at a much larger distance ($D > 2$ Mpc, or $> 10 R_{\text{vir}}$) from the nearest galaxy compared to all other metal-line detections. According to [Danforth et al. \(2016\)](#), this O VI absorber was detected at the 3.4σ confidence level in only one line of the doublet; no other metal transitions were detected despite the high $S/N \approx 30$ of the COS spectrum. No other absorber has anywhere near this level of uncertainty to its metal content; e.g., the next most remote O VI detection (in the 3C 263 sight line at $z_{\text{abs}} = 0.14075$, where $D = 0.62$ Mpc, or $2.8 R_{\text{vir}}$) is detected in several other metal ions, including both lines of the O VI doublet (see [Danforth et al. 2016](#)). Therefore, we doubt the reality of the HE0153-4520 O VI detection and do not consider it further.

To determine the maximum spread of metals more robustly, we show in [Figure 2](#) cumulative distribution functions (CDFs) for three different L_{lim} cuts in our galaxy survey for which the sampling is complete to $\geq 90\%$. Absorbers are included in each luminosity bin **only if** the galaxy survey is complete at or below L_{lim} .

The Anderson-Darling test was then used to determine the likelihood these two distributions, which are the nearest galaxy distances to O VI detections and non-detections, were randomly drawn from the same parent population. For the $L \geq L^*$ subsample, there is virtually no difference between the distributions of galaxies nearest to O VI detections and non-detections. The greatest contrast (p -value = 0.013) between the detections and non-detections is for the $L \geq 0.5 L^*$ subsample, for which the median distances to O VI detections were 0.5 Mpc and $2.79 R_{\text{vir}}$, and those for the non-detections were considerably larger, 0.74 Mpc and $4.23 R_{\text{vir}}$.

By using only those 15 absorbers whose surroundings were surveyed to at least $0.25 L^*$, we inspected the luminosities of the nearest galaxies: there are five $L < 0.5 L^*$ galaxies, ten $0.5 L^* \leq L < L^*$ galaxies, and zero at $L \geq L^*$. This is intriguing evidence that the primary contributor to spreading metals

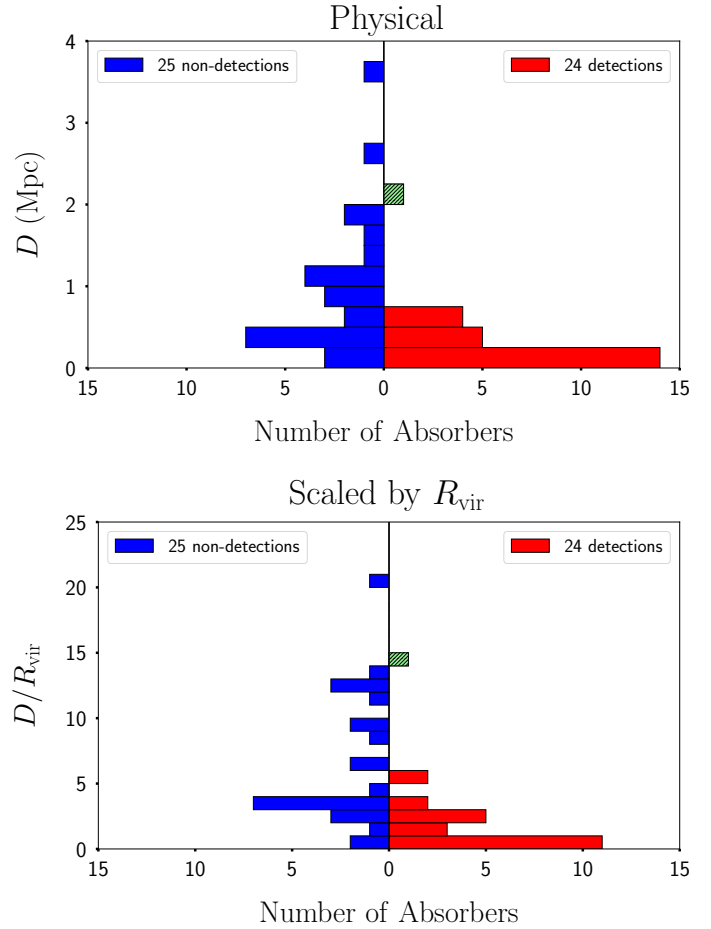


Figure 1. Histograms of O VI nearest galaxy distances in Mpc (*top*) and scaled nearest galaxy distances in units of R_{vir} (*bottom*). The red bars to the right represent the O VI detections, and the blue bars to the left are non-detections. No specific galaxy luminosity limit was applied for these data, thus utilizing all of the available galaxy redshift data we have in hand (i.e., columns 4-7 of [Table 2](#)). The green bar is the data point for the $z_{\text{abs}} = 0.13210$ absorber in the HE 0153-4520 sight line, which is a marginal O VI detection (see text).

into the CGM/IGM are galaxies somewhat fainter than L^* , similar to the Milky Way and M33.

To better compare our results for different L_{lim} , we scale the absorber-galaxy distance by the mean distance between galaxies of equal or greater luminosity ($\langle D_{\text{int}} \rangle$), given by the inverse cube root of the integral galaxy luminosity function. The SDSS luminosity function of [Montero-Dorta & Prada \(2009\)](#) with K -corrections from [Chilingarian, Melchior, & Zolotukhin \(2010\)](#) and [Chilingarian & Zolotukhin \(2012\)](#) were used to find values of: $\langle D_{\text{int}} \rangle = 5.96, 7.45, \text{ and } 10.4$ Mpc for $L_{\text{lim}} = 0.25, 0.5, \text{ and } 1 L^*$, respectively.

[Figure 3](#) compares the CDFs of the O VI detections for the three different L_{lim} subsamples. The median value of $D/\langle D_{\text{int}} \rangle$ for the $L_{\text{lim}} = 0.5 L^*$ subsample finds that these galaxies are ~ 20 times closer to absorbers than they are to

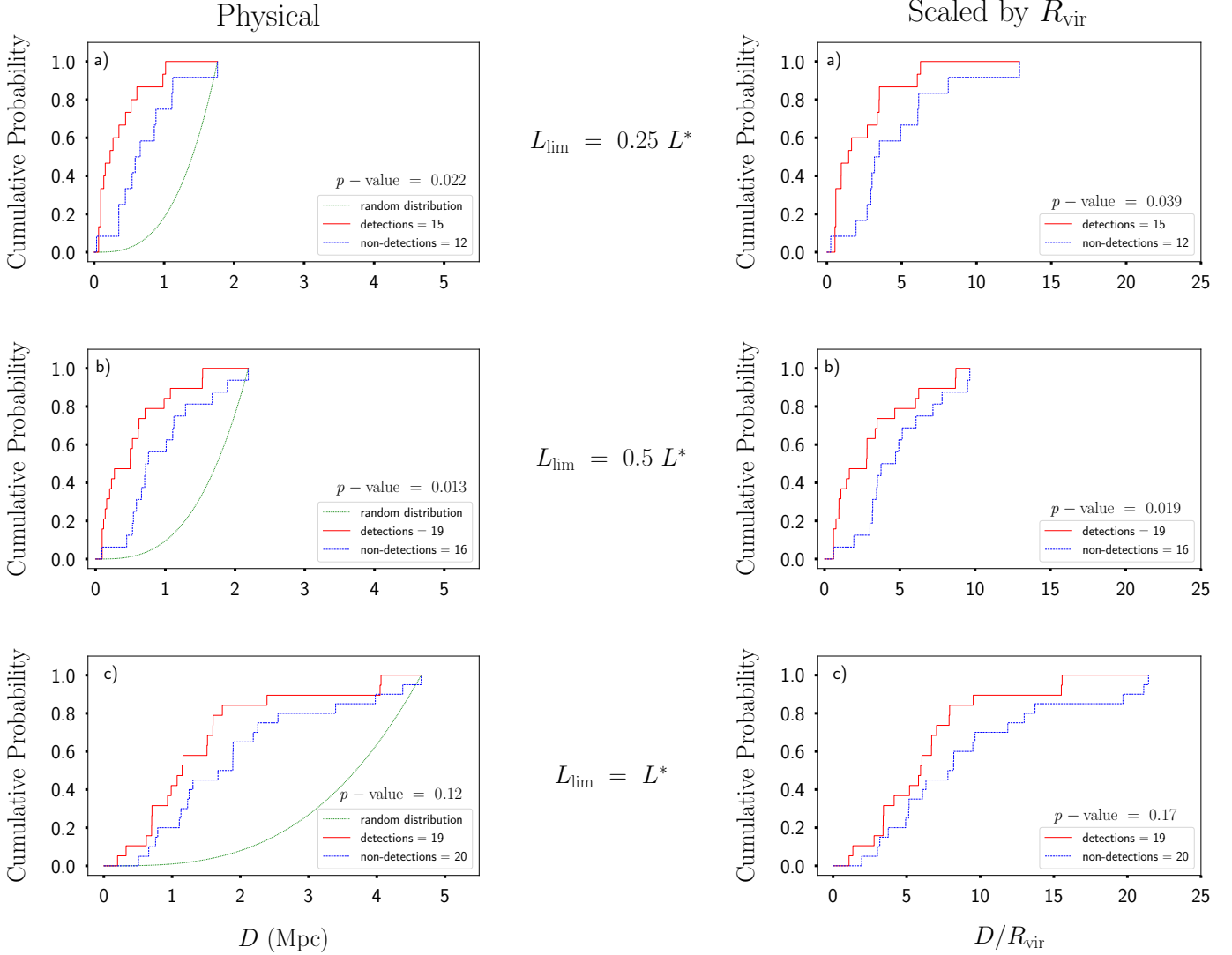


Figure 2. Cumulative distribution functions of O VI nearest galaxy distances (*left*) and distances scaled by R_{vir} (*right*). The solid red lines represent the O VI detections, the dashed blue lines are O VI non-detections, and the dotted green lines represent a random distribution of galaxies within a similar volume. The different panels (*a-c*) show the limiting luminosities of $0.25 L^*$, $0.5 L^*$, and $1 L^*$. All panels show a p -value found by the Anderson-Darling test, used to compare the distributions of O VI detections to non-detections.

other $L \geq 0.5 L^*$ galaxies. Clearly, O VI absorbers are tightly correlated with sub- L^* galaxies.

4. SUMMARY OF RESULTS AND DISCUSSION

Based on high-S/N, high-resolution FUV spectroscopy for samples of approximately two dozen low- z O VI absorption-line detections and non-detections, we find that O VI is not detected beyond a physical distance of ~ 0.6 Mpc, or $\sim 5 R_{\text{vir}}$ from the nearest galaxy. These results are in good agreement with those found by [Stocke et al. \(2006\)](#), who reported a spread of O VI to a maximum physical distance of ~ 800 kpc, or 3.5 - $5 R_{\text{vir}}$ from $L \geq L^*$ galaxies. More recently, [Johnson, Chen, & Mulchaey \(2015\)](#) reported O VI detections at 1 - $3 R_{\text{vir}}$ around galaxies of luminosities $L > 0.1 L^*$ at $z < 0.4$. Also, the correlation lengths found here are similar to those found by [Finn et al. \(2016\)](#) in a large, statistical study of low- z O VI

absorbers. Since these other recent studies use *HST/COS* FUV spectra of comparable or lesser S/N as the present study, these conclusions are all limited to $Z \geq 0.1 Z_{\odot}$; lower metallicity gas may be more pervasive in the IGM at both low- and high- z (e.g., [Aguirre, Schaye, & Theuns 2002](#)) than as measured here.

By creating subsamples defined by L_{lim} , we find evidence that O VI absorbers are more tightly correlated with $L < L^*$ galaxies than $L \geq L^*$ galaxies. Specifically, using only those absorbers with galaxy surveys complete $0.25 L^*$, we find that $2/3$ of O VI absorbers studied have nearest galaxies in the 0.5 - $1 L^*$ range. This result suggests that the majority of metals expelled into the CGM/IGM originate in sub- L^* galaxies.

The hypothesis that O VI absorbers are associated primarily with low-luminosity galaxies was originally proposed by

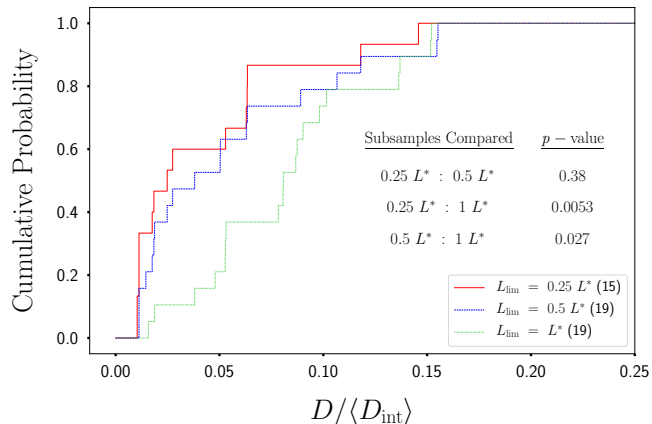


Figure 3. Cumulative distribution functions of O VI nearest galaxy distances scaled by the mean distances between galaxies of similar or greater luminosity. The red, blue, and green lines show the results for $L_{\text{lim}} = 0.25, 0.5,$ and $1 L^*$, respectively. The Anderson-Darling p -values comparing the subsamples are shown in the figure.

Tumlinson & Fang (2005) based on the dN/dz of O VI absorption systems, a hypothesis that was supported by our first galaxy-absorber study (Stocke et al. 2006). Later, Prochaska et al. (2011) made a similar suggestion based on their galaxy survey work, specifically identifying sub- L^* galaxies as the primary associated galaxies for low- z Ly α and metal-line systems. More recently, a very deep galaxy survey ($L \geq 0.01 L^*$) by Burchett et al. (2016) found C IV absorption associated primarily with galaxies at $L \geq 0.3 L^*$. The present study adds significantly to the intriguing speculation that CGM/IGM metals come primarily from sub- L^* galaxies.

Theoretical studies suggest that $L > L^*$ galaxies are too massive to allow metal-enriched gas to easily escape beyond R_{vir} while true dwarfs may eject too little gas *in toto* to be major contributors to CGM/IGM “metal pollution”. Since the sub- L^* galaxy population possesses bulk metallicities of a few tenths solar values (Tremonti et al. 2004), which is comparable to the absorber metallicities found for photoionized CGM absorbers (Stocke et al. 2013; Werk et al. 2014; Keeney et al. 2017), outflows escaping from these modest mass galaxies would not require significant dilution by more pristine gas to be observed as low- z CGM metal-line systems.

This study shows that O VI is not spread beyond distances comparable to a small galaxy group (1-2 Mpc in diameter). From this perspective, these results support the hypothesis that galaxy groups evolve nearly as “closed boxes” for chemical evolution. While relatively pristine ($Z < 0.1 Z_{\odot}$) gas can be accreted by a galaxy group, the metal-enriched gas expelled by the member galaxies does not appear to escape from the group, given the maximum distances that O VI absorbers are found from their plausible associated galaxy. This may be due to the somewhat deeper potential well of a galaxy group compared to an individual galaxy and/or to greater mass-loading as gas traverses the group.

Differences in the observed numbers of sub- L^* galaxies in galaxy groups (Zabludoff & Mulchaey 2000) could create different metallicity evolution histories between groups. This may contribute to the substantial width observed in the mass-metallicity relationship (Tremonti et al. 2004).

Only a small fraction of the O VI absorbers studied here are at temperatures hot enough to require collisional ionization, rather than photoionization; e.g., Savage et al. (2014) found 25% of aligned O VI absorbers (and only 1/6 of all O VI absorbers in their sample) have inferred $T \geq 10^5$ K. This fraction would amount to only ≤ 4 O VI absorbers in this sample. Therefore, this study does **not** address O VI absorption arising in warm-hot gas which may be associated with entire galaxy groups (Stocke et al. 2014).

This work was supported by NASA grants NNX08AC146 and NAS5-98043 to the University of Colorado at Boulder for the *HST*/COS project. CTP, JTS, and BAK gratefully acknowledge support from NSF grant AST1109117.

Facilities: AAT (AA Ω), Blanco (HYDRA, MOSAIC), FUSE, HST (COS), MMT (Hectospec), Sloan, WIYN (HYDRA), WIYN:0.9m (MOSAIC)

REFERENCES

- Aguirre, A., Schaye, J., & Theuns, T. 2002, *ApJ*, 576, 1
- Alam, S., Albareti, F. D., Allende Prieto, C., et al. 2015, *ApJS*, 219, 12
- Binney, J., & Tremaine, S. 1987, *Galactic dynamics*
- Bordoloi, R., Fox, A. J., Lockman, F. J., et al. 2017, *ApJ*, 834, 191
- Burchett, J. N., Tripp, T. M., Bordoloi, R., et al. 2016, *ApJ*, 832, 124
- Cen, R., & Ostriker, J. P. 1999, *ApJ*, 514, 1
- Chen, H.-W., Lanzetta, K. M., Webb, J. K., & Barcons, X. 1998, *ApJ*, 498, 77
- Chilingarian, I. V., Melchior, A.-L., & Zolotukhin, I. Y. 2010, *MNRAS*, 405, 1409
- Chilingarian, I. V., & Zolotukhin, I. Y. 2012, *MNRAS*, 419, 1727
- Colless, M., Dalton, G., Maddox, S., et al. 2007, *VizieR Online Data Catalog*, 7250
- Côté, B., Martel, H., Drissen, L., & Robert, C. 2012, *MNRAS*, 421, 847
- Danforth, C. W., Keeney, B. A., Tilton, E. M., et al. 2016, *ApJ*, 817, 111
- Davé, R., Finlator, K., & Oppenheimer, B. D., 2011, *MNRAS*, 416, 1354
- Davé, R., Hernquist, L., Katz, N., & Weinberg, D. H. 1999, *ApJ*, 511, 521
- Ferland, G. J., Korista, K. T., Verner, D. A., et al. 1998, *PASP*, 110, 761
- Finn, C. W., Morris, S. L., Tejos, N., et al. 2016, *MNRAS*, 460, 590
- Green, J. C., Froning, C. S., Osterman, S., et al. 2012, *ApJ*, 744, 60
- Hayward, C. C., & Hopkins, P. F. 2017, *MNRAS*, 465, 1682
- Hopkins, P. F., Torrey, P., Faucher-Giguère, C.-A., Quataert, E., & Murray, N. 2016, *MNRAS*, 458, 816
- Johnson, S. D., Chen, H.-W., & Mulchaey, J. S. 2015, *MNRAS*, 449, 3263
- Jones, D. H., Read, M. A., Saunders, W., et al. 2009, *MNRAS*, 399, 683
- Keeney, B. A., Danforth, C. W., Stocke, J. T., et al. 2006, *ApJ*, 646, 951
- Keeney, B. A., Stocke, J. T., Danforth, C. W., et al. 2017, *ApJS*, 230, 6
- Montero-Dorta, A. D., & Prada, F. 2009, *MNRAS*, 399, 1106
- Muratov, A. L., Kereš, D., Faucher-Giguère, C.-A., et al. 2015, *MNRAS*, 454, 2691
- . 2017, *MNRAS*, 468, 4170
- Oppenheimer, B. D., Davé, R., Katz, N., Kollmeier, J. A., & Weinberg, D. H. 2012, *MNRAS*, 420, 829
- Pagel, B. E. J. 2009, *Nucleosynthesis and Chemical Evolution of Galaxies*
- Prochaska, J. X., Weiner, B., Chen, H.-W., Mulchaey, J., & Cooksey, K. 2011, *ApJ*, 740, 91
- Prochaska, J. X., Werk, J. K., Worseck, G., et al. 2017, *ApJ*, 837, 169
- Savage, B. D., Kim, T.-S., Wakker, B. P., et al. 2014, *ApJS*, 212, 8
- Shull, J. M. 2014, *ApJ*, 784, 142
- Stocke, J. T., Danforth, C. W., Shull, J. M., Penton, S. V., & Giroux, M. L. 2007, *ApJ*, 671, 146
- Stocke, J. T., Keeney, B. A., Danforth, C. W., et al. 2013, *ApJ*, 763, 148
- Stocke, J. T., Penton, S. V., Danforth, C. W., et al. 2006, *ApJ*, 641, 217
- Stocke, J. T., Keeney, B. A., Danforth, C. W., et al. 2014, *ApJ*, 791, 128
- Tremonti, C. A., Heckman, T. M., Kauffmann, G., et al. 2004, *ApJ*, 613, 898
- Tumlinson, J., & Fang, T. 2005, *ApJL*, 623, L97
- Tumlinson, J., Thom, C., Werk, J. K., et al. 2011, *Science*, 334, 948
- Veilleux, S., Cecil, G., & Bland-Hawthorn, J. 2005, *ARA&A*, 43, 769
- Werk, J. K., Prochaska, J. X., Tumlinson, J., et al. 2014, *ApJ*, 792, 8
- Zabludoff, A. I., & Mulchaey, J. S. 2000, *ApJ*, 539, 136